

A comparison of the electronic structure and optical plasmons in Cs_x , Cs_x shells and C_{60}Cs_x clusters

Jens Ekengren,¹ Johan Sjöholm,¹ Daniel Östling,¹ Arne Rosén,¹ and David Tománek²

¹*Department of Physics, Göteborg University, SE-412 96 Göteborg, Sweden*

²*Physics and Astronomy Department,*

Michigan State University, East Lansing, Michigan 48824-2320

(Dated: March 29, 2006)

Abstract

We calculate the electronic structure and collective electronic excitations in Cs_x , Cs_x shells and Cs_x covered C_{60} clusters. The ground state properties of these systems are described using the Local Density Approximation, and the electronic excitations by the Random Phase Approximation. The jellium approximation underlying our calculations correctly predicts the magic numbers and optical excitation spectra in these systems, in agreement with experimental results.

PACS numbers: 36.40.Gk, 78.66.Tr, 33.60.-q, 73.22.-f

I. INTRODUCTION

Alkali metal clusters are very interesting systems, which allow us to observe the gradual transition in the electronic structure from isolated atoms to bulk metals. The large degree of delocalization of valence electrons, characteristic of alkali metals, is an important property of these clusters. This delocalization shows up most dramatically in the appearance of magic numbers corresponding to shell orbitals encompassing the entire cluster¹⁻⁴. The electronic response of these systems is particularly interesting in that it shows one of the characteristics of a macroscopic plasmon, namely a large fraction of the oscillator strength concentrated in a narrow frequency range⁵. We will address this collective mode as the cluster plasmon mode⁵. In contrast to the prediction of the classical Mie theory as applied to metal spheres, this collective mode is typically 30% lower in frequency for small clusters, and shows a pronounced size dependence⁶.

Recently, surface plasmons and plasmons of metal shells have come in to interest with the development of surface plasmon resonance (SPR) measurements, in which one uses the shift of the surface plasmon of small particles as they are exposed to different reactants. This technique has also been applied in medicine, using mostly noble metal clusters and shells, to detect very small concentrations of various molecules⁷.

In the following, we calculate the ground state electronic structure of small homogeneous Cs clusters, Cs shells, and Cs coated C₆₀ clusters using the density functional theory (DFT). We will use the calculated value of the gap between the highest occupied (HOMO) and lowest unoccupied molecular orbital (LUMO) to judge the relative stability of these systems. Using the Random Phase Approximation (RPA), we will then predict and compare the optical spectra of these systems. We will finally compare our results to optical absorption spectra of mass selected clusters.

II. THEORY

A. Density functional calculations of the electronic eigenstates

We calculate the electronic structure for spherical potentials using the density functional theory within the Local Density Approximation (LDA)^{9,10}. The charge density $\rho(\mathbf{r})$ in the electronic ground state, and the corresponding total energy of the system $E[\rho(\mathbf{r})]$, are

determined by solving self-consistently the set of Kohn-Sham equations¹⁰

$$\left[-\frac{1}{2}\nabla^2 + V_{eff}(\mathbf{r}) \right] \psi_i(\mathbf{r}) = \varepsilon_i \psi_i(\mathbf{r})$$

$$\rho(\mathbf{r}) = \sum_{\mathbf{i}}^{\text{occ}} |\psi_{\mathbf{i}}(\mathbf{r})|^2 . \quad (1)$$

The effective potential V_{eff} in the local density approximation is given by

$$V_{eff}(\mathbf{r}) = V_{ion}(\mathbf{r}) + V_H(\rho(\mathbf{r})) + V_{xc}(\rho(\mathbf{r})) , \quad (2)$$

where V_{ion} is the ionic background potential, V_H is the Hartree potential, and V_{xc} is a local potential describing the effect of exchange and correlation. In the present work, we use the Vosko-Wilk-Nusair parameterization for the Ceperley-Alder formulation¹¹ of V_{xc} ,

$$V_{xc}(r_s) = V_x(r_s) + V_c(r_s) = -4\left(\frac{3\rho}{8\pi}\right)^{1/3} - \frac{A}{3} \frac{1+b_1 r_s^{1/2}}{1+b_1 r_s^{1/2} + b_2 r_s + b_3 r_s^{3/2}} +$$

$$+ A \left[\ln \frac{r_s}{X(r_s)} + \frac{2b}{Q} \tan^{-1} \frac{Q}{2\sqrt{r_s+b}} - \frac{bx_o}{X(x_o^2)} \left(\ln \frac{(\sqrt{r_s}-x_o)^2}{X(r_s)} + \frac{2(b+2x_o)}{Q} \tan^{-1} \frac{Q}{2\sqrt{r_s+b}} \right) \right] \quad (3)$$

where

$$Q = \sqrt{4c - b^2} \quad (4)$$

and

$$X(z) = z + b\sqrt{z} + c \quad (5)$$

with the values¹¹ $A = 0.0621814$, $b_1 = 9.81379$, $b_2 = 2.82224$, $b_3 = 0.736412$, $x_o = -0.10498$, $b = 3.72744$ and $c = 12.9352$.

The most accurate approach to determining the electronic states of clusters involves considering the discrete atomic structure. This could be achieved in a self-consistent manner using LDA with a Linear Combination of Atomic Orbitals (LCAO) basis. However, the large number of atoms needed to describe a large cluster makes a simplified approach more attractive. In the following, we focus on the electronic structure arising from the interacting valence electrons and replace the point charges of the individual ions by a uniform volume charge in the jellium approximation.

The jellium background is shaped as a solid sphere in the case of Cs_x clusters, or as a spherical shell in the case of Cs covered C_{60} molecules and free-standing Cs shells. The inner radius of the shell matches the minimum of the charge density for the bare C_{60} . The charge density of the jellium is given by the free electron radius, defined by $r_s(\mathbf{r}) = [3/4\pi\rho(\mathbf{r})]^{1/3}$. We use the value $r_s = 5.62 a_0$ for Cesium¹². Since Cs has one valence electron, the outer radii of all clusters with x atoms are constructed so that the total charge of the jellium is x .

1. *Eigenvalue problem in systems with spherical symmetry*

The jellium potential associated with the ionic background charge of a spherical cluster of radius R is

$$V_{ion}(r) = \begin{cases} -\frac{Z}{R} \left(\frac{3}{2} - \frac{1}{2} \left(\frac{r}{R} \right)^2 \right) & r \leq R \\ -\frac{Z}{r} & r > R. \end{cases}$$

The jellium potential of a spherical shell having the inner radius R_1 and outer radius R_2 is

$$V_{ion}(r) = \begin{cases} -Z \frac{3}{2} \frac{R_2^2 - R_1^2}{R_2^3 - R_1^3} & r \leq R_1 \\ -Z \frac{3rR_2^2 - 2R_1^3 - r^3}{2r(R_2^3 - R_1^3)} & R_1 < r \leq R_2 \\ -\frac{Z}{r} & r > R_2. \end{cases}$$

The eigenfunctions of the Kohn-Sham operator can be factorized into radial and angular parts as

$$\psi_{nlm}(r, \theta, \varphi) = R_{nl}(r) Y_{lm}(\theta, \varphi). \quad (6)$$

We now construct a spherical box of large but finite radius R to confine the electronic states. The discretization of the spectrum due to the finite value of R is minimized for sufficiently large values of R . The most challenging problem is the determination of the radial wave function $R_{nl}(r)$, which we solve by first using the standard substitution $R_{nl}(r) = P_{nl}(r)/r$. The Kohn-Sham Eq. (1) leads to a new equation for $P_{nl}(r)$,

$$\left[-\frac{1}{2} \frac{\partial^2}{\partial r^2} + \frac{l(l+1)}{2r^2} + V_{eff}(r) \right] P_{nl}(r) = \varepsilon_{nl} P_{nl}(r). \quad (7)$$

As we outline in the following section, we have solved this differential equation numerically for different systems.

2. *Numerically stable technique to solve the eigenvalue problem*

A numerical solution of the differential equation (7) for the radial function $P_{nl}(r)$ using a standard point-and-shoot method¹⁴ is known to be unreliable due to numerical instability. To solve this differential equation, we adopt a technique by Salomonson and Öster⁸, originally developed for atoms, to clusters. The objective is to determine the eigenfunction $P_{nl}(r)$ on a linear grid of N points r_1, \dots, r_N , separated by a constant distance h . To evaluate

the kinetic term in the radial equation (7), we use the symmetric five-point formula for the second-order derivative of a function $P_{nl}(r)$,

$$\frac{\partial^2 P(r)}{\partial r^2} = \frac{1}{12h^2}[-P(r-2h) + 16P(r-h) - 30P(r) + 16P(r+h) - P(r+2h)] + O(h^4). \quad (8)$$

Substituting the expression (8) in Eq. (7) leads to a set of N coupled linear equations for $P_{nl}(r_i)$ that can be formulated as an eigenvalue problem,

$$(A + D) \mathbf{P}_{nl} = \varepsilon \mathbf{P}_{nl}. \quad (9)$$

Determining the eigenvector $\mathbf{P} = (P_{nl}(r_1), P_{nl}(r_2), \dots, P_{nl}(r_N))$ in Eq. (9) is equivalent to solving Eq. (7) on the radial grid. In matrix representation, the operator A is diagonal, with its elements given by

$$A_{ii} = \frac{l(l+1)}{2r_i^2} + V_{ion}(r_i) + V_H(r_i) + V_{xc}(r_i), \quad (10)$$

where $i = 1, 2, \dots, N$. D is the symmetric band matrix obtained from Eq. (8), given by

$$D = -\frac{1}{24h^2} \begin{pmatrix} -30 & 16 & -1 & 0 & 0 & \cdots & 0 \\ 16 & -30 & 16 & -1 & 0 & \cdots & 0 \\ -1 & 16 & -30 & 16 & -1 & \cdots & -1 \\ \vdots & \vdots & \vdots & \vdots & \vdots & \ddots & 16 \\ 0 & 0 & 0 & 0 & -1 & 16 & -30 \end{pmatrix}. \quad (11)$$

We require $A + D$ to be symmetric in order to obtain a real eigenvalue ε in Eq. (9) and a radial eigenfunction $P_{nl}(r)$ that is real and doubly differentiable everywhere inside the sphere. The above form of D implies that the wave functions vanish outside the grid, i.e. all electrons are contained in the spherical box. The asymptotic behavior of $P_{nl}(r)$ in the region close to the origin, $P_{nl}(r) \propto r^l$, has to be enforced, while still keeping the matrix D symmetric⁸. To achieve this, we focus on the matrix elements D_{11} , D_{12} , D_{21} and D_{22} . The $A + D$ matrix can be symmetrized by extending the radial axis to the left of the first grid point. To do so, we use the ansatz

$$\begin{aligned} P_{nl}(r_0) &= \alpha \left[\frac{P_{nl}(r_0)}{P_{nl}(r_1)} \right] P_{nl}(r_1) + (1 - \alpha) \left[\frac{P_{nl}(r_0)}{P_{nl}(r_2)} \right] P_{nl}(r_2) \\ P_{nl}(r_{-1}) &= \left[\frac{P_{nl}(r_{-1})}{P_{nl}(r_1)} \right] P_{nl}(r_1) \end{aligned} \quad (12)$$

for the function values at the grid points r_{-1} and r_0 preceding the first grid point r_1 . The function value ratios occurring in Eq. (12) are determined using the appropriate asymptotic behavior of $P_{nl}(r)$. The free parameter α is then chosen so that $D_{12} = D_{21}$.

We note that the total number of eigenstates is determined by the rank N of the matrices A and D in Eq. (9), which is related to the number of the radial grid points and not the total number of electrons. Consequently, this approach can be used to determine also the unoccupied states, which are the basis of calculations determining the collective response of these systems.

B. Random Phase Approximation

The RPA approach uses a summation of possible excitation paths to incorporate all processes that dissipate the incoming energy. The excitation energy spectrum calculated using the RPA approach differs from that of the free electron approximation, since the latter ignores relaxation of electrons that were not initially excited.

The RPA equation, which determines the excitation energy spectrum $\hbar\omega_\lambda$, has the form¹⁵⁻¹⁷

$$\begin{pmatrix} A^\lambda & B^\lambda \\ -B^{\lambda*} & -A^{\lambda*} \end{pmatrix} \begin{pmatrix} X^\nu \\ Y^\nu \end{pmatrix} = \hbar\omega_\nu \begin{pmatrix} X^\nu \\ Y^\nu \end{pmatrix}. \quad (13)$$

Here, the submatrices A and B are defined by the matrix elements of the two-body interaction, coupled by angular momentum, such that

$$\begin{aligned} & A^\lambda(ph, p'h') - (\epsilon_{n_p, l_p} - \epsilon_{n_h, l_h}) \delta_{l_p, l_{p'}} \delta_{l_h, l_{h'}} \delta_{n_p, n_{p'}} \delta_{n_h, n_{h'}} = \\ & = 2I^\lambda(ph', hp') (-1)^{l_p + l_{p'}} \frac{[(2l_p + 1)(2l_h + 1)(2l_{p'} + 1)(2l_{h'} + 1)]^{1/2}}{2\lambda + 1} \times \\ & \quad \times \begin{pmatrix} l_h & \lambda & l_p \\ 0 & 0 & 0 \end{pmatrix} \begin{pmatrix} l_{h'} & \lambda & l_{p'} \\ 0 & 0 & 0 \end{pmatrix} = \\ & = (-1)^\lambda B^\lambda(ph, p'h'), \end{aligned} \quad (14)$$

with

$$\begin{aligned} & I^\lambda(ph', hp') = \\ & = \int r_1^2 dr_1 r_2^2 dr_2 R_{n_p, l_p}(r_1) R_{n_{h'}, l_{h'}}(r_2) V(r_1, r_2; \lambda) R_{n_h, l_h}(r_1) R_{n_{p'}, l_{p'}}(r_2). \end{aligned} \quad (15)$$

The radial part of the interaction between two particles, to the multipole order λ , is

$$V(r_1, r_2; \lambda) = e^2 \frac{r_{<}^\lambda}{r_{>}^{\lambda+1}} + \frac{dV_{xc}[\rho]}{d\rho} + \frac{\delta(r_1 - r_2)}{r_1^2} \frac{2\lambda + 1}{4\pi}, \quad (16)$$

where $r_{<}$ ($r_{>}$) is the smaller (larger) value of r_1 and r_2 .

In Eqs. (14) and (15), n_i corresponds to the total number of radial nodes, and l_i the orbital angular momentum of the wave function describing the particle (p) or hole (h) state. The total angular momentum - the multipole order - of the excitation is λ . In the present work, we are only interested in dipole excitations, described by $\lambda = 1$.

In this case, the matrix elements of the dipole operator,

$$M(E\lambda; \mu) = \sqrt{\frac{4\pi}{2\lambda + 1}} er^\lambda Y_{\lambda\mu}(\hat{\mathbf{r}}), \quad (17)$$

are reduced to

$$\langle \nu || M(E\lambda) || 0 \rangle = \sum_{ph} [X_{ph}^{\nu*}(\lambda) + (-1)^\lambda Y_{ph}^{\nu*}(\lambda)] \langle p || M(E\lambda) || h \rangle \quad (18)$$

and the oscillator strength f_ν is defined by

$$f_\nu = \frac{4m_e}{3N_e \hbar^2 e^2} E_\nu | \langle \nu || M(E1) || 0 \rangle |^2. \quad (19)$$

The total oscillator strength that this calculated with RPA obeys the TRK sum rule. This means that the sum of the oscillator strengths is the same for the unscreened (free) electron-hole excitations and for excitations calculated using the RPA.

III. RESULTS

A. Ground-state properties

High relative stability of clusters has often been correlated with a large HOMO-LUMO gap. In the following, we consider clusters with the HOMO-LUMO gap exceeding 0.1 eV. For Cs_x clusters, these cluster sizes are $x = \mathbf{2}, \mathbf{8}, \mathbf{18}, \mathbf{20}, \mathbf{34}, 40, \mathbf{58}, 68, 90, \mathbf{92}, 106, 132, \mathbf{138}, 168, \mathbf{186}, 196, 198, 232, \mathbf{254}, 268, 306, \mathbf{338}, 398, 428, 438, 440$. In case of spherical Cs shells with an inner radius $r_{inner} = 5.0 \text{ \AA}$, describing alkali covered C_{60}Cs_x clusters, the cluster sizes with a large HOMO-LUMO gap are $x = \mathbf{2}, \mathbf{8}, \mathbf{18}, \mathbf{32}, 50, \mathbf{52}, \mathbf{58}, 80, \mathbf{90}, 116, \mathbf{130}, 162, 180, \mathbf{186}, 230, \mathbf{252}, 304, \mathbf{330}, 332, \mathbf{428}, \mathbf{438}, 484$. In this list, we have denoted cluster sizes, which are sometimes called ‘‘magic’’ due to their extra stability, in bold face.

B. Optical response

As a direct result of RPA calculations, we obtain the energies of the dipole allowed transitions, $\hbar\omega$, and the corresponding oscillator strengths. Folding these RPA oscillator strengths with a Lorentzian of the form

$$L(\omega) = \frac{A\Gamma}{2\pi((\omega - \omega_p)^2 + (\frac{\Gamma}{2})^2)} \quad (20)$$

yields the optical response function at a finite temperature. A is used to normalize the area under the curve to unity for every ω_p , thus conserving the relative strengths of the excitations. For all figures presented here, we used either $\Gamma = 0.2$ eV or $\Gamma = 0.2$ meV. $\Gamma = 0.2$ eV gives a realistic optical response, as can be seen in room temperature experiments. The narrower Lorentzian with $\Gamma = 0.2$ meV is used to show the actual oscillator peaks and their strengths in more detail.

Figures 1 to 4 depict the dielectric response as the frequency-dependent oscillator strength in Cs_x clusters and Cs_x shells with $x=8, 18, 58, 138, 186$ and 306 atoms.

Results presented in Fig. 1, comparing free and RPA response of small clusters, show that the main effect of RPA is to blue shift the oscillator frequency, with little effect on the oscillator strength. The $\hbar\omega < 1$ eV feature in the free response is red shifting as the clusters grow larger, reflecting increasing band broadening. In the RPA spectrum, this feature appears as the Mie plasmon at $\hbar\omega \gtrsim 1.5$ eV and blue shifts towards 2 eV with increasing cluster size, in agreement with experimental data.

Fig. 2 shows the change of the dielectric response when a cavity is placed at the center of a Cs_x cluster. The cavity has a radius of $r_{inner} = 3.57$ Å in order to mimic the presence of a C_{60} fullerene in the center²⁴. In other words, the created structure is a shell of Cs atoms surrounding an inactive C_{60} core.

In order to compare our results with experimental data from mass selected clusters¹⁹, Fig. 3 and Fig. 4 compare the oscillator strength of neutral and ionized clusters. For the sake of simple comparison, neutral and charged clusters with the same number of valence electrons have been placed side by side.

Calculations have also been performed with a C_{60} fullerene contained inside a Cs_x shell. Within the rigid band model, we will consider a complete transfer of the 240 valence electrons from C_{60} to the Cs_x shell. The free and RPA dielectric response of C_{60}Cs_x are compared in

Fig. 5 for $x=8, 18, 58$ and 130 .

The dielectric response of hollow Cs_x shells and $C_{60}Cs_x$ clusters is compared in Fig. 6. We note an additional peak at 18 eV, described as the σ -plasmon of C_{60} , in systems that contain a C_{60} in the core. On the extended energy abscissa, used in Figs. 5 and 6, this mode appears in addition to the 2 eV mode, associated with the Cs clusters and shells. The details of the 2 eV plasmon in Cs_x with and without a C_{60} at the core, shown in Fig. 7, suggest that the effect of C_{60} on the optical spectra is moderate at low coverages $x \lesssim 60$, and further diminishes with increasing value of x .

IV. CONCLUSIONS

We have calculated optical properties of various Cs clusters, both solid spheres and spherical shells, using LDA and RPA code adapted for spherical symmetry. “Magic” cluster sizes, occurring more abundantly in the mass spectra, have been also found to exhibit a large HOMO-LUMO gap in our calculations, thus confirming the adequacy of our computational approach.

Our results generally agree with trends found in earlier studies. We clearly demonstrate a blue shift of the plasmon mode with increasing cluster size. We also identified a broadening of the plasmon peak, when the uniform cluster is transformed to a hollow shell.

Analyzing the optical properties of ionized clusters suggests that their optical spectra should lie very close to those of neutral clusters with the same size. In other words, optical spectra of mass-selected ionized clusters should compare well with calculated spectra for the same cluster size regardless of ionization level, provided that the total number of electrons in the different systems is the same.

In general, we find a remarkable agreement in terms of plasmon peak positions and widths when comparing our results to observed optical spectra for Cs clusters^{19,20}. We find that the presence of C_{60} at the center of the cluster does change the optical properties of the system. Obviously, the optical spectra of $C_{60}Cs_x$ clusters and Cs_x shells become rather similar with increasing number of Cs atoms, but some minor differences in the spectra remain even in moderately large systems.

Systems containing the C_{60} in the core exhibit a strong feature around 18 eV, which is the σ plasmon of the C_{60} molecule²⁵. In $C_{60}Cs_x$ clusters with very many Cs atoms, the effect

of the C_{60} σ plasmon becomes negligible.

Comparing details of the 2 eV plasmon spectra in $C_{60}Cs_x$ clusters and hollow Cs_x shells, depicted in Fig. 7, suggest that presence of C_{60} in the core causes a general broadening of the plasmon feature, caused by coupling between the electrons in the Cs and the carbon shells. We note that the broader peak is also in better agreement with experimental data, suggesting that using a hollow Cs_x shell as a model of Cs covered C_{60} clusters does not provide a very accurate description of the optical response. Some of the changes in the optical spectra, caused by the presence of C_{60} , may be addressed by considering the 240 valence electrons on the enclosed C_{60} , even though they are strongly bound to the carbon cage.

V. ACKNOWLEDGEMENTS

The authors acknowledge financial support from the Swedish Research Council, VR. DT was partly funded by the NSF NIRT grants DMR-0103587, ECS-0506309, and NSF NSEC grant EEC-425826.

-
- ¹ W. A. de Heer, W. Knight, M. Chou and M. Cohen, *Solid State Physics* **40**, 93 (1987).
 - ² S. Bjornholm *et al.*, *Phys. Rev. Lett.* **65**, 1627 (1990).
 - ³ W. A. de Heer, *Rev. Mod. Phys.* **65**, 611 (1993).
 - ⁴ M. Brack, *Rev. Mod. Phys.* **65**, 677 (1993).
 - ⁵ W. A. de Heer, K. Selby, V. Kresin, J. Masui, M. Vollmer, A. Chatelain, and W. D. Knight, *Phys. Rev. Lett.* **59**, 1805 (1987).
 - ⁶ J. H. Parks and S. A. McDonald, *Phys. Rev. Lett.* **62**, 2301 (1989).
 - ⁷ N. Halas, *MRS Bulletin* **30**, 362 (2005).
 - ⁸ S. Salomonson and P. Öster, *Phys. Rev. A* **40**, 5559 (1989).
 - ⁹ P. Hohenberg and W. Kohn, *Phys. Rev. B* **136**, 864 (1964).
 - ¹⁰ W. Kohn and L.J. Sham, *Phys. Rev. A* **140**, 1133 (1965).
 - ¹¹ S. H. Vosko, L. Wilk and M. Nusair, *Can. J. Phys.* **58**, 1200 (1980).
 - ¹² N.W. Ashcroft and N.D. Mermin, *Solid State Physics* (Brooks/Cole, New York, 1976) p. 5.

- ¹³ J.D. Jackson, *Classical Electrodynamics*, Second Ed., (John Wiley and Sons, New York, 1975).
- ¹⁴ S.E. Koonin, *Computational Physics* (The Benjamin/Cummings Publishing, Menlo Park, 1986).
- ¹⁵ D.J. Rowe, *Nuclear Collective Motion*, (Methuen, London, 1970).
- ¹⁶ D.J. Rowe, Rev. Mod. Phys. **40**, 153 (1968).
- ¹⁷ C. Yannouleas and R.A. Broglia, Phys. Rev. A **44**, 5793 (1991).
- ¹⁸ M. Springborg, S. Satpathy, N. Malinowski, U. Zimmermann, and T.P. Martin, Phys. Rev. Lett. **77**, 1127 (1996).
- ¹⁹ S. Frank, N. Malinowski, F. Tast, M. Heinebrodt, I.M.L. Billas, and T.P. Martin, Z. Phys. D **40**, 250 (1997).
- ²⁰ H. Fallgren and T.P. Martin, Chem. Phys. Lett. **168**, 233 (1990).
- ²¹ T.P. Martin, U. Zimmermann, N. Malinowski, M. Heinebrodt, S. Frank and F. Tast, Phys. Scripta **T66**, 38 (1996).
- ²² H. Fallgren, K.M. Brown, and T.P. Martin, Z. Phys. D **19**, 81 (1991).
- ²³ E. Koch and O. Gunnarsson, Phys. Rev. B **54**, 5168 (1996).
- ²⁴ P.Mierzynski and K. Pomorski, Eur. Phys. J. D **21**, 311 (2002).
- ²⁵ George F. Bertsch, Aurel Bulgac, David Tománek and Yang Wang, Phys. Rev. Lett. **67**, 2690 (1991).

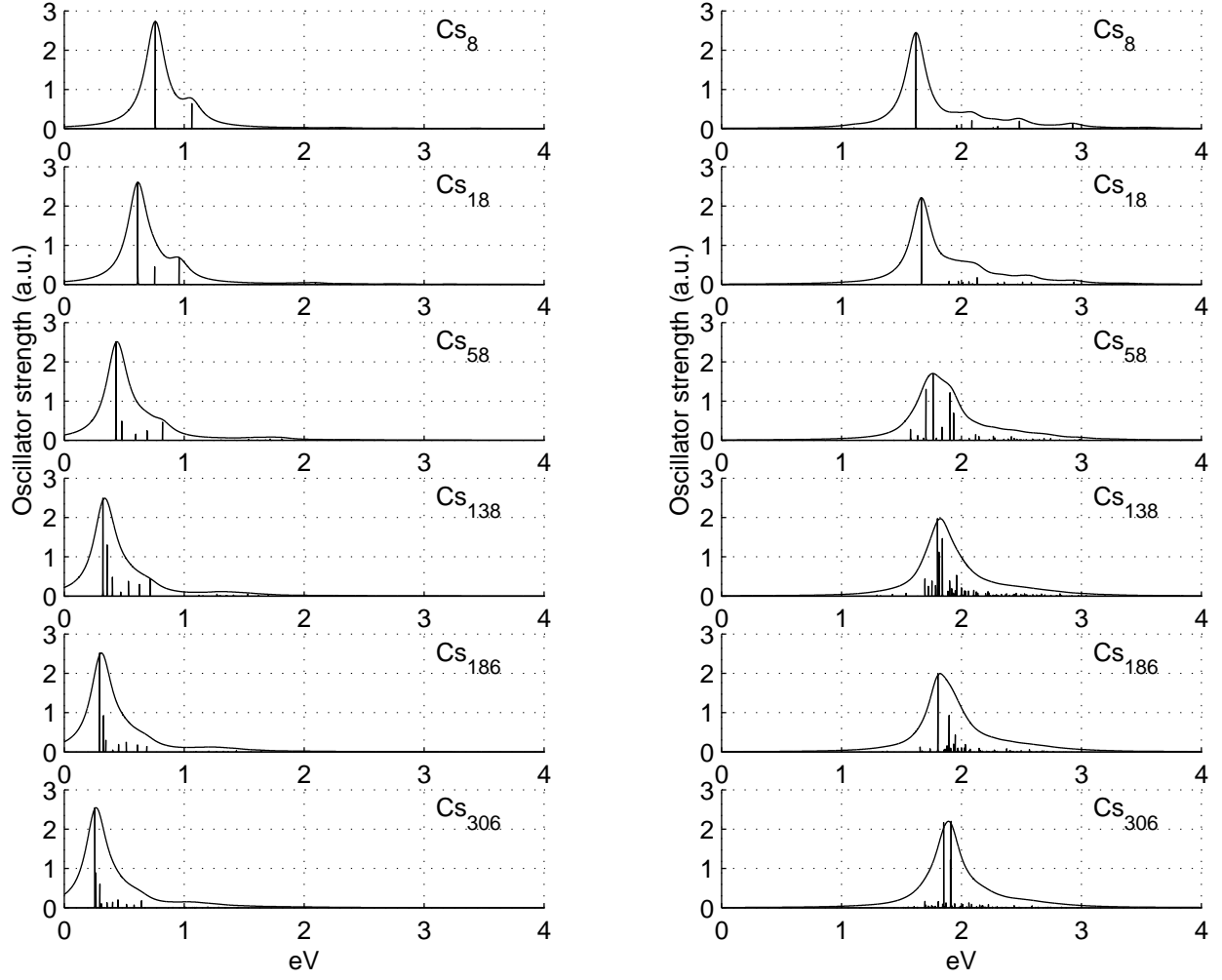


FIG. 1: Oscillator strengths for Cs_x clusters with $x=8, 18, 58, 138, 186$ and 306 atoms. Results based on free response, shown on the left, are compared to results based on RPA response, shown on the right.

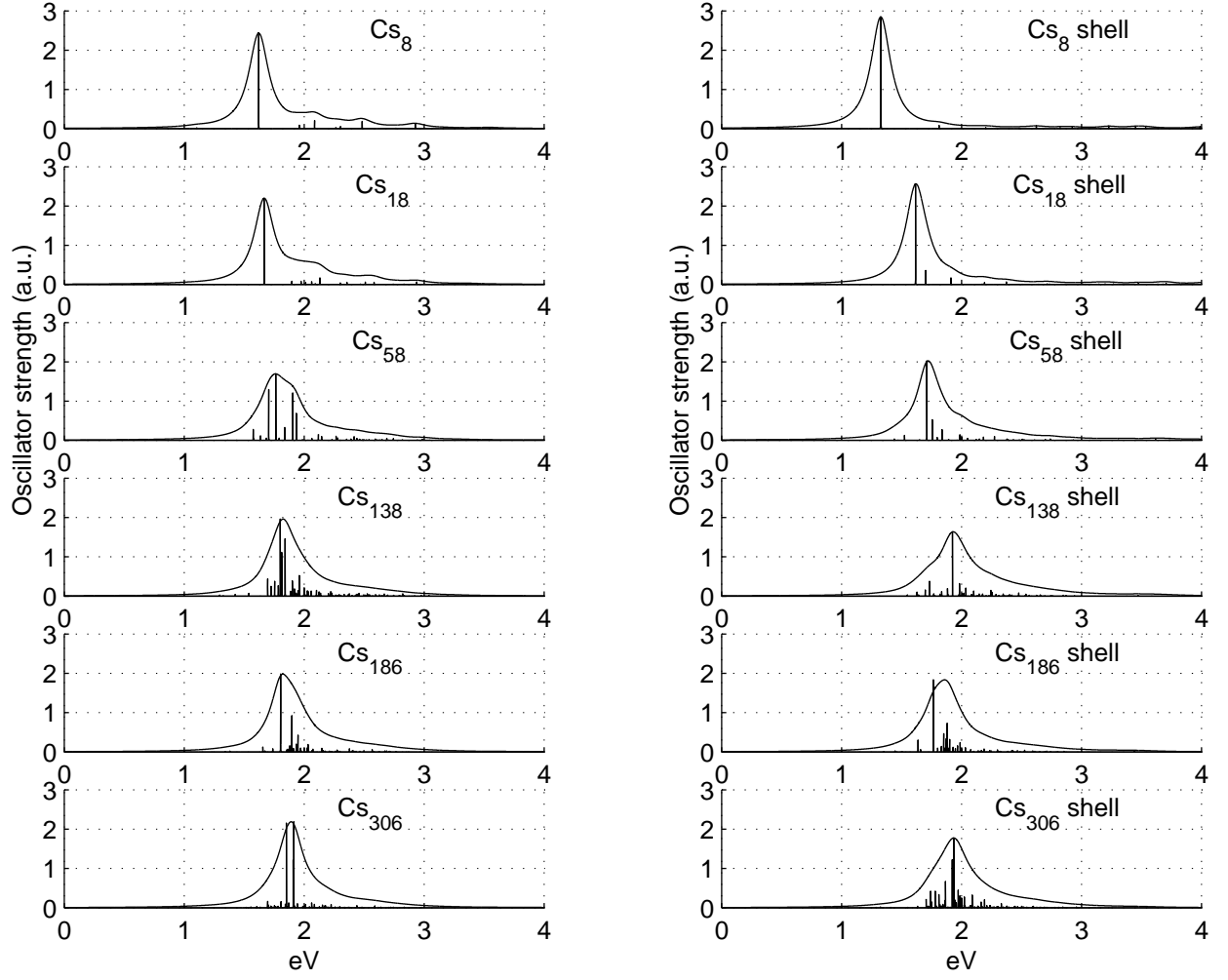


FIG. 2: RPA oscillator strengths of homogeneous Cs_x clusters, shown on the left, and hollow Cs_x shells, shown on the right.

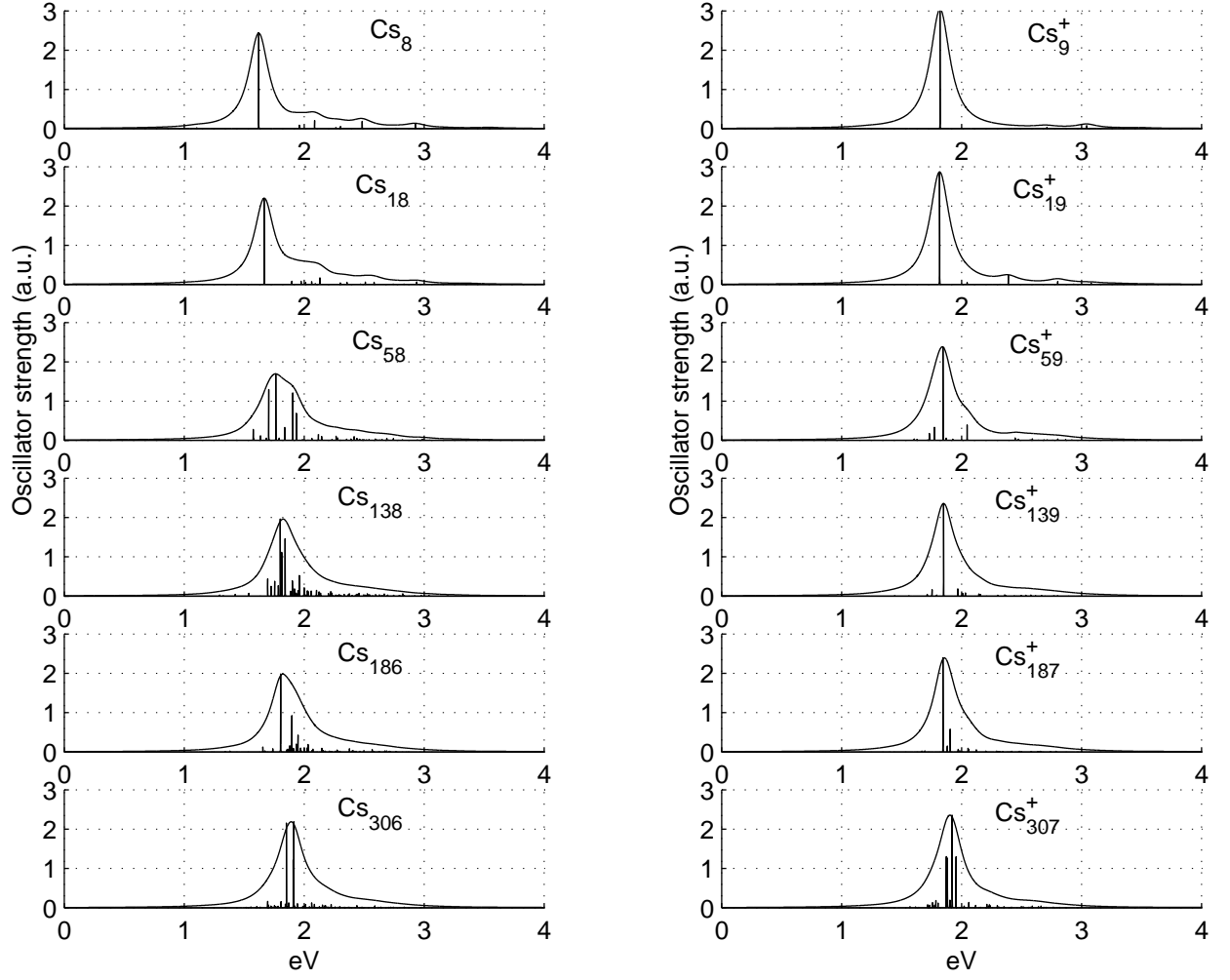


FIG. 3: RPA oscillator strengths of neutral Cs_x clusters (left column) and singly ionized Cs_{x+1}^+ clusters (right column).

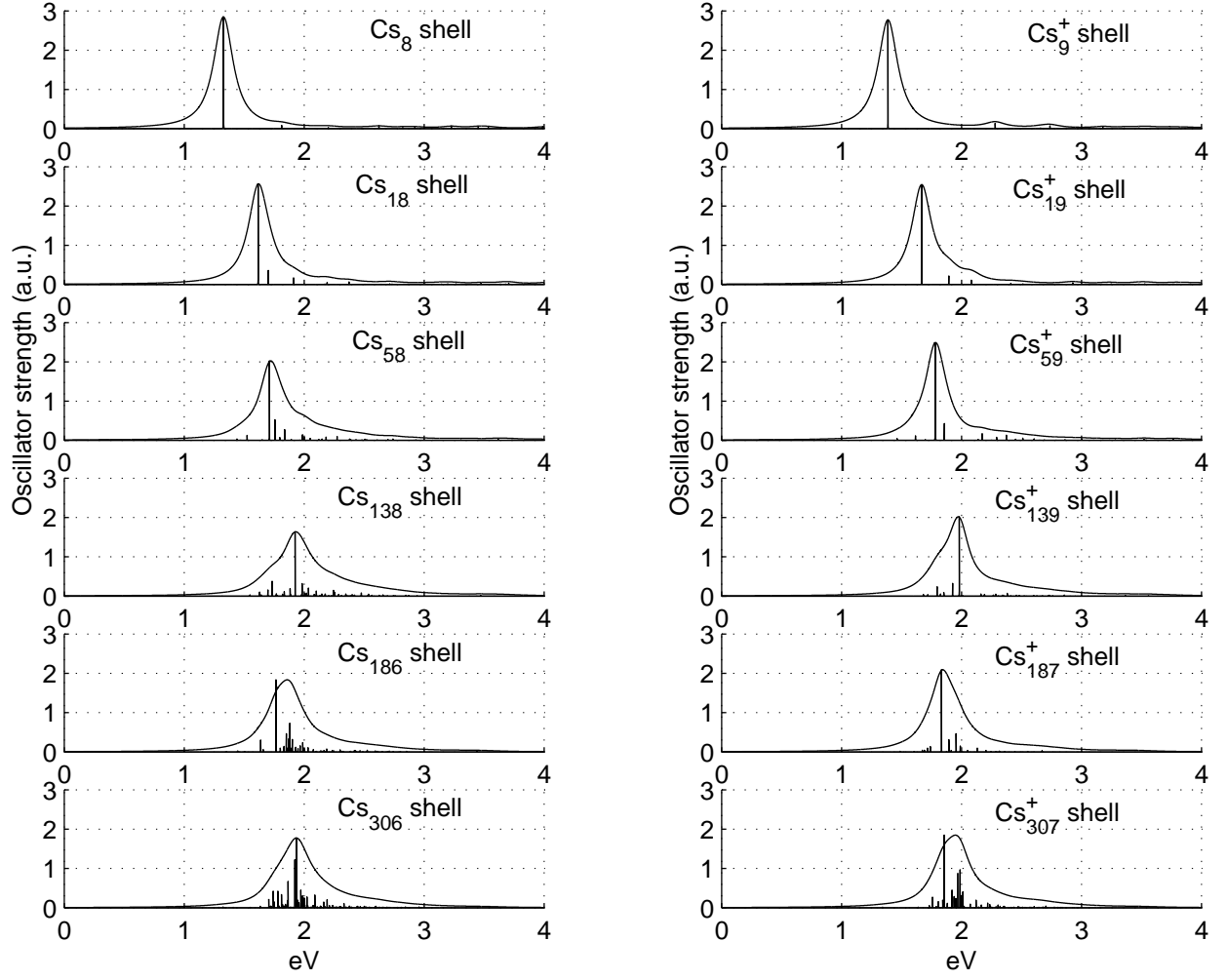


FIG. 4: RPA oscillator strengths of neutral Cs_x shells (left column) and singly ionized Cs_{x+1}^+ shells (right column).

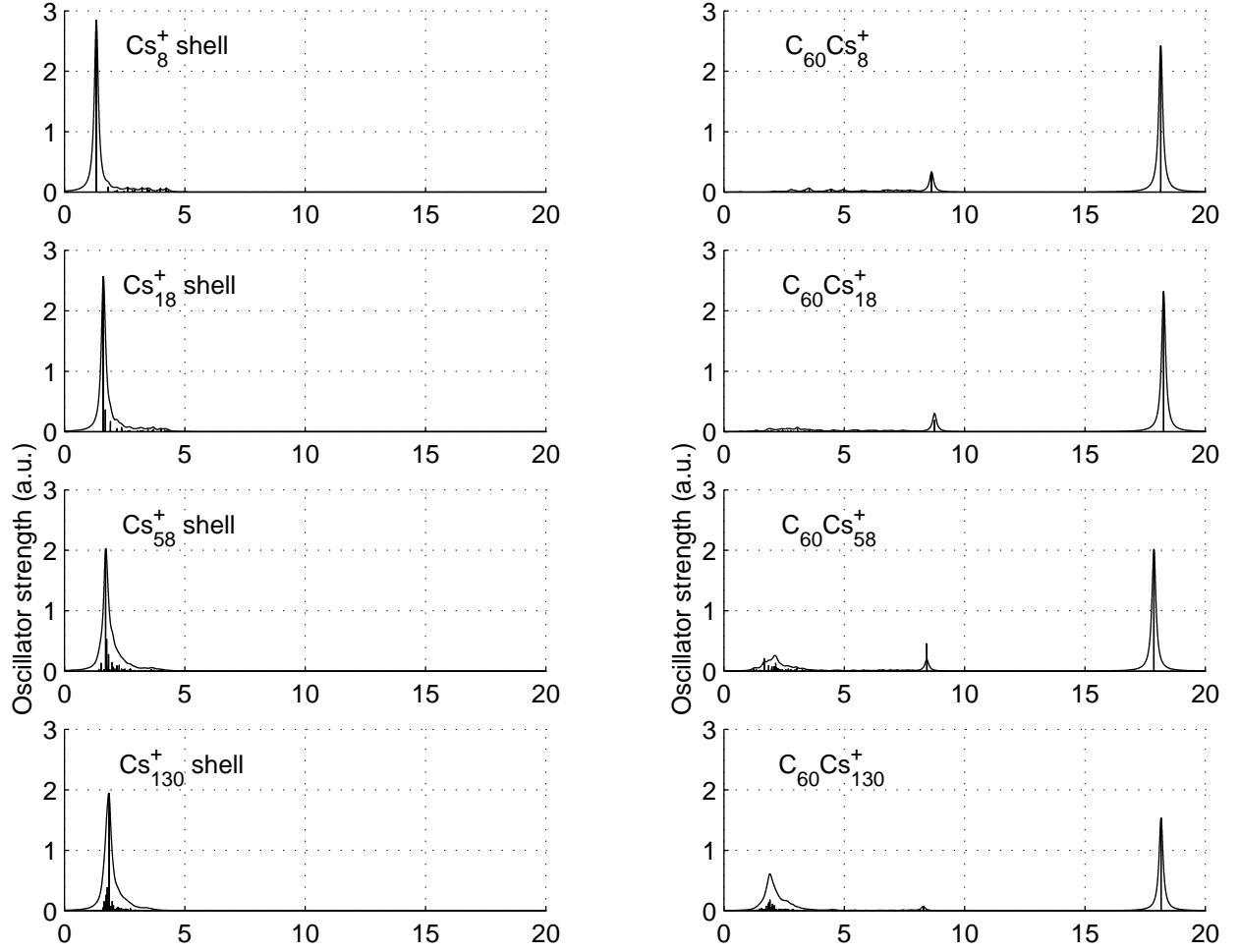


FIG. 5: Oscillator strengths for singly ionized $C_{60}Cs_x^+$ clusters with $x=8, 18, 58$ and 130 atoms. Results based on free response, shown on the left, are compared to results based on RPA response, shown on the right.

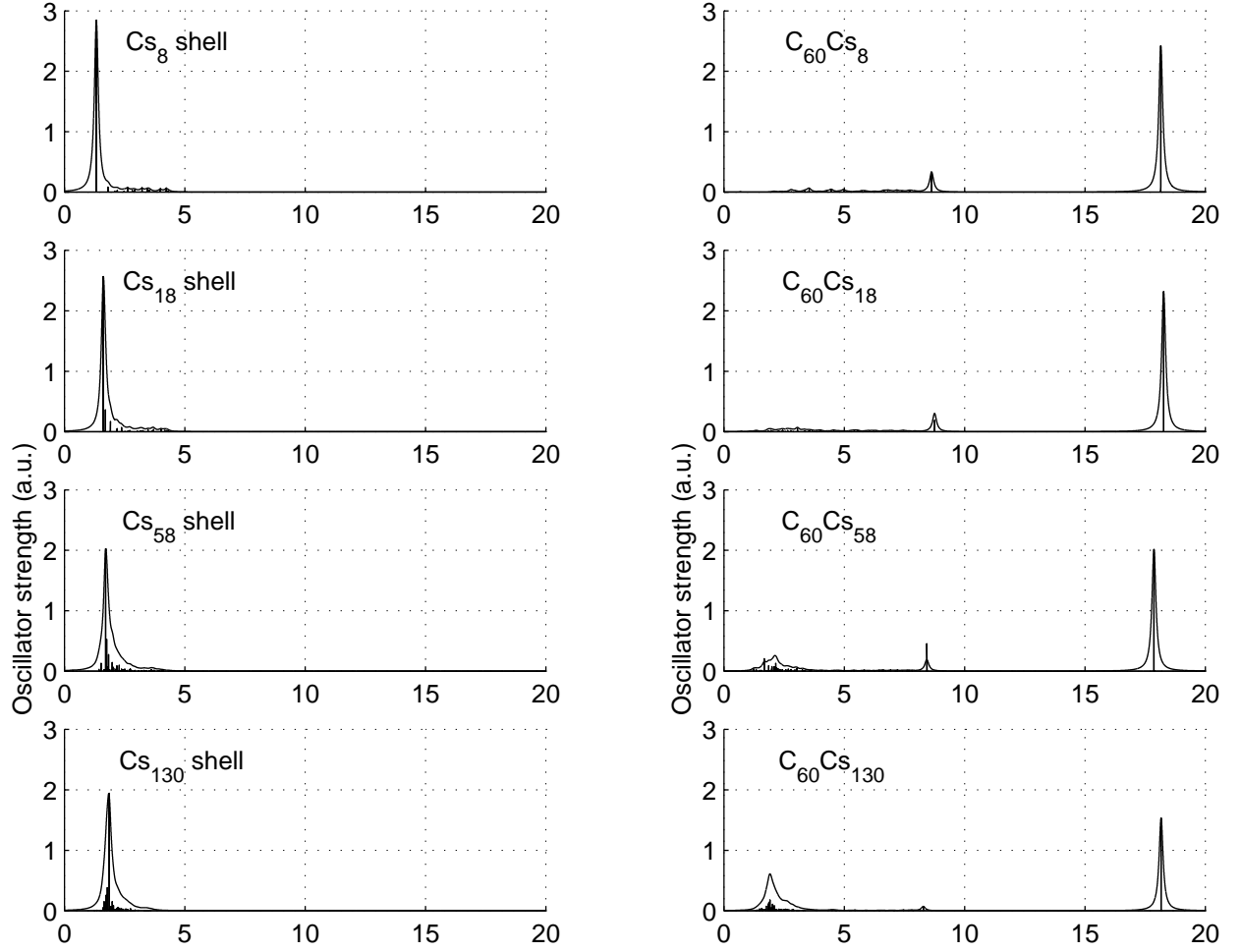


FIG. 6: RPA oscillator strengths of Cs_x shells (left column) and $C_{60}Cs_x$ clusters (right column) with $x=8, 18, 58$ and 130 atoms.

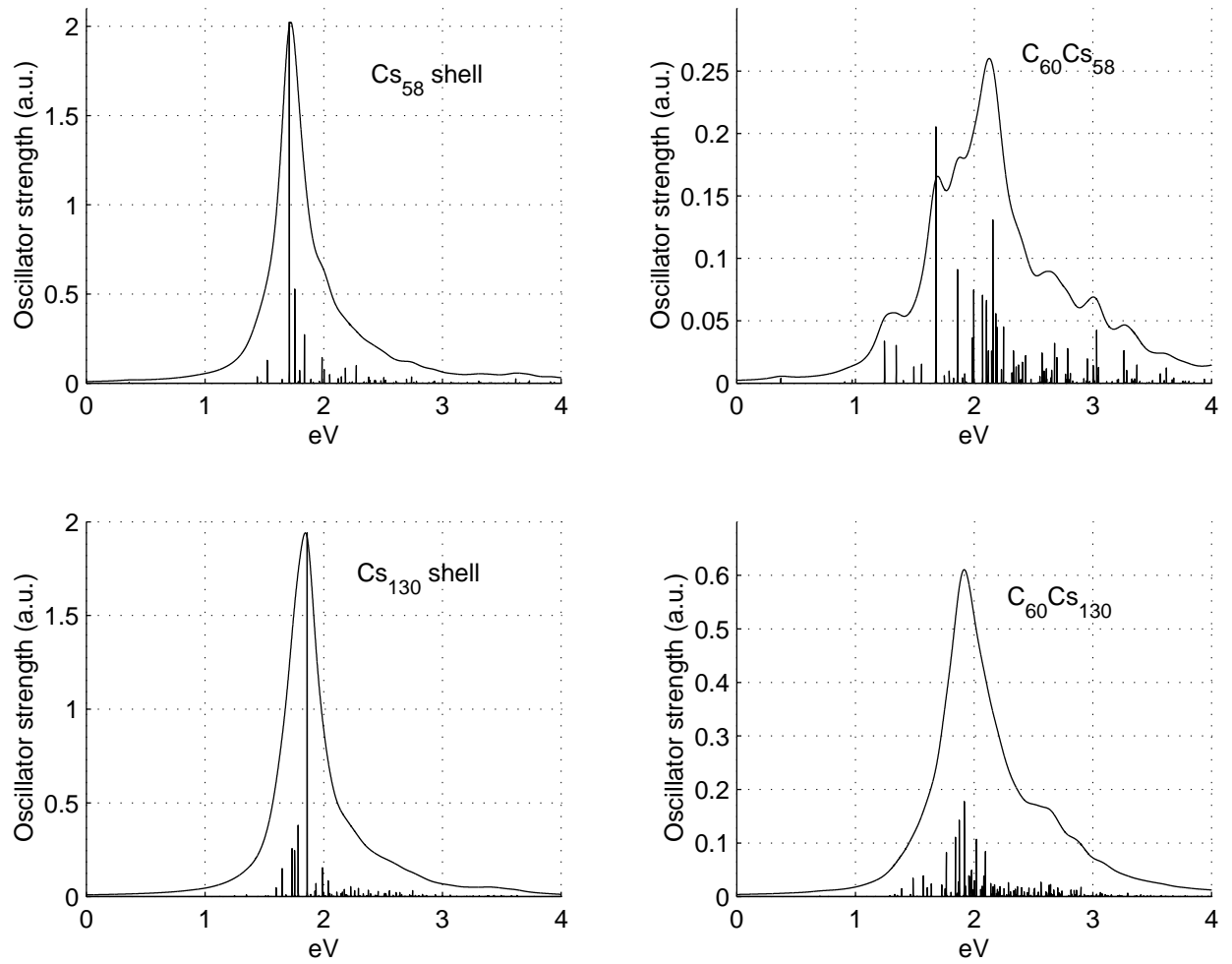


FIG. 7: Details of Fig. 6, depicting the RPA oscillator strengths near the 2 eV peak in Cs_x shells (left column) and C_{60}Cs_x clusters (right column) with $x=58$ and 130 atoms.